Science of the Total Environment 646 (2019) 121–133

Contents lists available at ScienceDirect

Science of the Total Environment

journal homepage: www.elsevier.com/locate/scitotenv

Evaluating the role of particle size on urban environmental geochemistry of metals in surface sediments

Jessica Unda-Calvo [a,*], Estilita Ruiz-Romera [a], Silvia Fdez-Ortiz de Vallejuelo [b], Miren Martínez-Santos [a], Ainara Gredilla [c]

[a] Department of Chemical and Environmental Engineering, University of the Basque Country (UPV/EHU), Plaza Ingeniero Torres Quevedo 1, Bilbao 48013, Basque Country, Spain
[b] Department of Analytical Chemistry, Faculty of Science and Technology, University of the Basque Country (UPV/EHU), E-8940 Leioa, Basque Country, Spain
[c] Department of Applied Chemistry, Faculty of Chemistry, University of the Basque Country (UPV/EHU), E-2018 San Sebastián, Basque Country, Spain

HIGHLIGHTS

- Non-destructive and invasive methodologies for surface sediment characterization
- Metal geochemistry variation in particle size distribution controls availability.
- Natural processes and human activities are sources of available metals.
- Higher ecological risk was identified in the dry compared to the wet season.

GRAPHICAL ABSTRACT

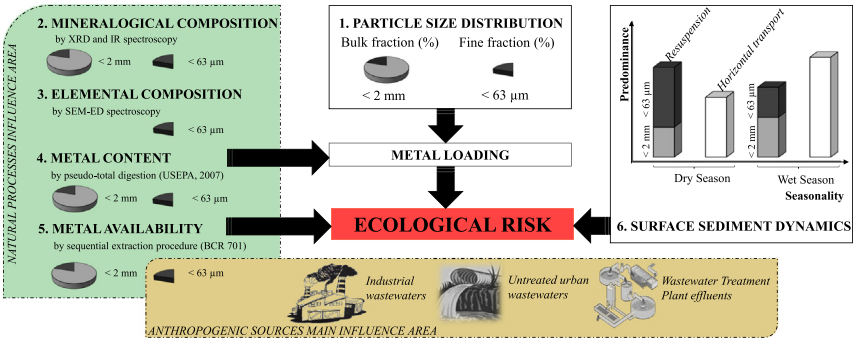

ARTICLE INFO

Article history:
Received 28 March 2018
Received in revised form 13 July 2018
Accepted 13 July 2018
Available online 24 July 2018

Editor: Xinbin Feng

Keywords:
Surface sediment
Particle size, geochemistry
Ecological and health risk
Urban environment

ABSTRACT

In this study, non-destructive techniques (X-ray Diffraction, Infrared and Scanning Electron Microscopy with Energy Dispersive spectroscopies) and invasive procedures (pseudo-total and sequential metal extraction methodologies) were used to highlight the significance of evaluating different particle sizes of sediments for assessing the potential environmental and health implications of metal geochemistry in an urban ecosystem.

The variability in composition and properties between bulk (<2 mm) and fine (<63 µm) fractions influenced the availability, and by extension, the toxicity of metals. Indeed, the fine fraction presented not only higher metal pseudo-contents, but also greater available metal percentages. Besides the larger surface area per unit of mass and the high content of clay minerals, it was observed that it was principally Fe/Mn oxyhydroxides that favour adsorption of metals on the fine surface sediments. However, although we demonstrated that the origin of metals in the bulk surface sediments was predominantly lithogenic, use of the <2 mm fraction proved to be a useful tool for identifying different sources of available metals throughout the Deba River catchment. Specifically, discharges of untreated industrial and urban wastewaters, and even effluents from wastewater treatment plants were considered to greatly increase the health risk associated with metal availability. Finally, an evaluation of sediment dynamics in different hydrological conditions has highlighted the role played by each particle size as a vector of metal transport towards the coastal area. While resuspension of fine surface sediments notably induced significantly higher particulate metal concentrations in water during the dry season, resuspension of bulk surface sediments and, fundamentally, downstream transport of suspended particulate matter became more relevant and lowered the ecological risk during the wet season. Greater attention therefore needs to be paid to the new

* Corresponding author.
E-mail address: jessica.unda@ehu.eus (J. Unda-Calvo).

https://doi.org/10.1016/j.scitotenv.2018.07.172

hydrological scenarios forecast to result from climate change, in which longer seasons with low river discharges are forecast.

1. Introduction

According to World Population Prospects (United Nations, 2017 Revision), the world's population is projected to grow from nearly 7.6 billion in 2017 to 8.6 billion in 2030. Intense development of human activity, driven by demographic growth, will greatly impact environmental quality and by extension, human health (Ghanem, 2018). Several studies have addressed the impact of urbanization on the quality of aquatic environments, including high loadings of nutrient and microbial contaminants from both septic systems and wastewater treatment plants (WWTPs) (Carey et al., 2013; McGrane et al., 2014), volatile organic compounds from vehicular emissions (Mahbub et al., 2011) and metals, mainly from industrial or urban effluents (Gupta et al., 2010; Buzier et al., 2011), among others.

Sediment is a good indicator of pollution loads in rivers since it is subject to a continuous accumulation of pollutants, especially metals (Devesa-Rey et al., 2010; Bartoli et al., 2012). These contaminants are considered to pose a serious threat to ecological and human health because of their non-biodegradable, toxic and persistent nature, as well as their capacity to enter the food chain (Burghardt, 1994; van Kamp et al., 2003; Armitage et al., 2007). The percentage of total metal content in the sediment that is available for absorption into the systemic circulation system and that has a toxic impact on human health, will depend firstly on environmental availability (Lanno et al., 2004; Harmsen, 2007), which is in turn related to its chemical forms or types of binding (Saracoglu et al., 2009; Sungur et al., 2014). The physical and geochemical properties of sediments such as surface to volume ratio, mineralogical composition and organic matter are considered to influence chemical distribution of metals (Simpson and Batley, 2009; Campana et al., 2012; Saeedi et al., 2013; Zhang et al., 2014). However, particle size determines all these properties and, therefore, it is the cornerstone parameter (Maslennikova et al., 2012).

To date, numerous researchers have used different analytical techniques (X-ray Diffraction, Infrared and Scanning Electron Microscopy or Inductively Coupled Plasma) to individually investigate the grain size effect over: the mineralogical and elemental composition (Zhou et al., 2015) or the metal chemical speciation (Liang et al., 2018); as well as the mineralogical effect over the metal content (Xie et al., 2018). However, considering all these techniques as a whole may be more suitable to bind the particle size effect on the geochemistry of sediments with the metal accumulation, distribution and environmental impact.

In urban environments, geochemical patterns observed in different particle sizes of sediments help to differentiate the contribution to metal availability of non-anthropogenic sources from human activities (Chiprés et al., 2009). Indeed, sediment records the geochemical composition of the provenance bedrock and the intensity of chemical weathering and hydraulic sorting (Lapworth et al., 2012; Zhao and Zheng, 2015; Kirkwood et al., 2016; Darwish, 2017). During chemical weathering of the bedrock, water-soluble elements are chemically dissolved in water, whereas water-insoluble elements are physically transported by the water current (Zhao and Zheng, 2014). Consequently, despite the high adsorption capacity of minerals, the chemical dissolution of soluble ones might promote the availability of metals previously retained in their lattice.

Additionally, after elucidate the source and magnitude of available metals in each particle size, sediment dynamics become decisively important in addressing the ecological consequences of seasonal variations in river discharge. Indeed, the physical processes involved in sediment dynamics include erosion, transport, deposition, and resuspension (ICES, 2011), which are the result of interactions between several variables such as water discharge or grain size distribution (USEPA, 1999; Apitz, 2012). According to future climate change predictions, alterations in the seasonal precipitation (magnitude and duration) and, consequently, river flow variations are expected. Therefore, deeper knowledge into sediment dynamics will be crucial for a better estimation of metal environmental risk, based on the new hydrological scenarios.

The overall aim of this study is therefore to identify the relevance of analysing different particle sizes, as a more reliable reflection of the environmental geochemistry of metals in surface sediments from an urban catchment and the associated ecological and human health risk. The specific objectives were (i) to use different methodologies for mineralogical, elemental and metal characterization of surface sediments, (ii) to identify natural processes and/or sources of anthropogenic contamination influencing the environmental and health risk associated with the availability of metals in surface sediments, and (iii) to evaluate the influence of seasonality on physical mechanisms governing metal migration towards the coastal area. We hypothesized that combined analysis of different particle sizes of surface sediment will provide us more comprehensive and detailed information about the environmental geochemistry of metals in a catchment subjected to multiple pressures.

2. Materials and methods

2.1. Study area and sampling

The Deba River runs through the catchment (538 km^2) to the Bay of Biscay, receiving inflows from several tributaries, including the Ego and Oñati streams (Fig. 1). The geology of the catchment mainly consists of a succession of sedimentary rocks, predominantly an alternation of sandstones and mudstones in the northern and western part, marls in the central area, and limestones in the southern region. In contrast, igneous rocks dominate the area of confluence of the Ego tributary and the main river (Fig. 1A).

The Deba River catchment possesses certain characteristics which are distinctive of a typical urban environment. These include dense population, a relatively high level of productivity, primarily driven by non-agricultural activities, infrastructures, buildings, and an extensive motor transportation network (Wong et al., 2006; Fig. 1B).

Surface waters receive treated effluents from three wastewater treatment plants (Fig. 1B). The Apraitz (95,000 population equivalent (pe)) and Mekolalde (35,000 pe) WWTPs have been operating since 2007 and 2008, respectively. The Epele WWTP (90,000 pe) only came into continuous operation in May 2012; previously, organic-rich wastewaters from the towns of Arrasate and Oñati were discharged into the Deba River and Oñati stream. In June 2014, the sewer from Ermua-Eibar was also connected to the Apraitz WWTP and untreated urban wastewater (UWW) from these municipalities is no longer discharged into the Ego stream. However, according to data from Gipuzkoa Provincial Council, about 6773 $m^3\ y^{-1}$ of untreated industrial wastewater (IWW) from metal-working, the automotive industry, galvanising, smelting factories and electrical appliance manufacturers are also discharged into the Deba River and its tributaries (Martínez-Santos et al., 2015). In this context, surface sediments are characterized by having a high content of metals, nutrients and organic compounds, principally in areas of greatest urbanization and industrialization. Previous studies have shown that discharges of effluents from WWTPs and even IWW and UWW throughout the catchment are responsible for the declining quality of surface sediments, posing a potential risk for the ecosystem (Unda-Calvo et al., 2018) and for human health (Unda-

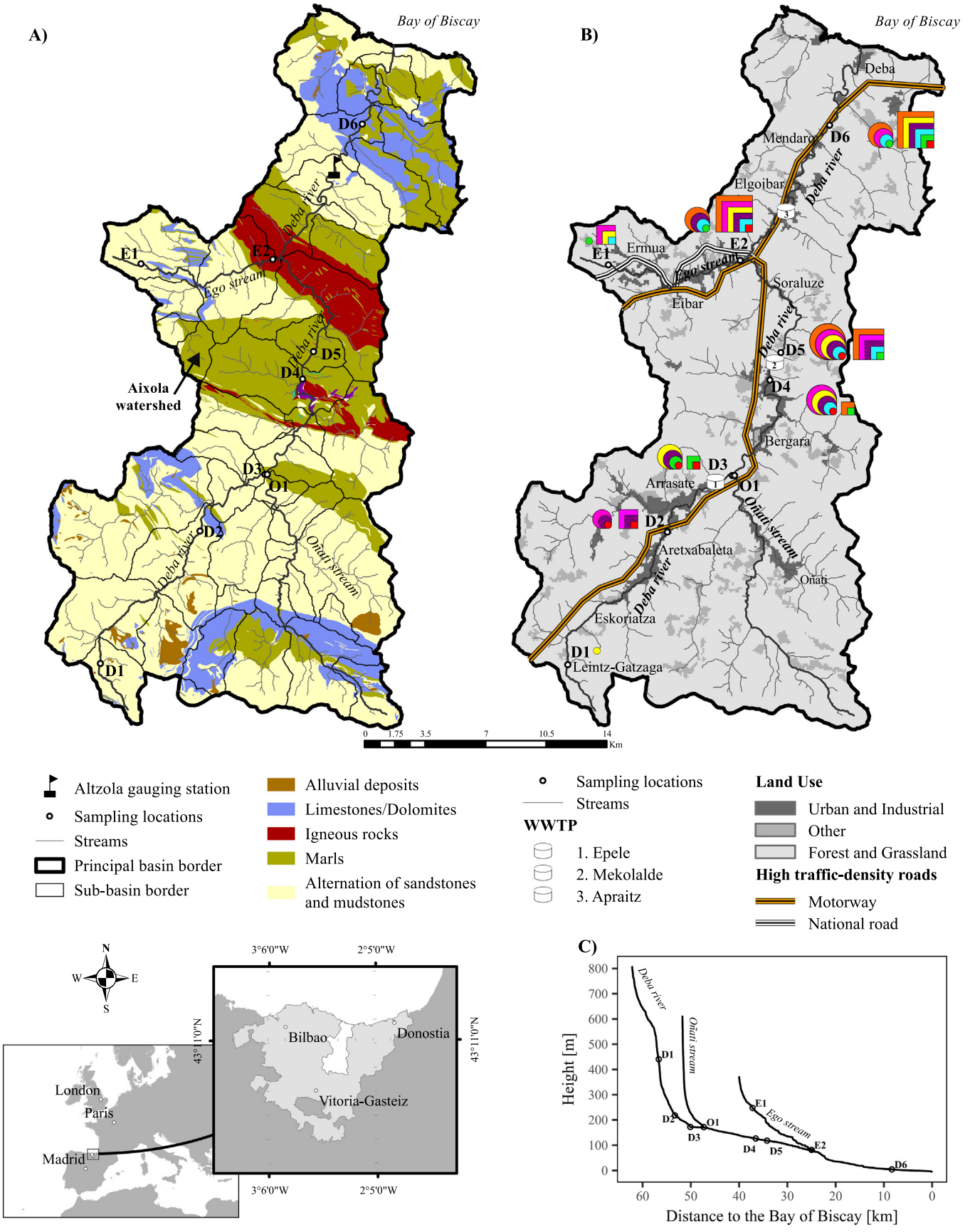

Fig. 1. Location of Deba River catchment, and (A) lithological map, (B) land use map, and (C) height profile. The sub-basin subdivision and the location of Altzola gauging station can be observed in (A). The sampling sites, the wastewater treatment plants (WWTPs) and high traffic-density roads are shown in (B). Circles and squares represent the anomalies (normalized-concentration > 1) shown by each metal (Fe: red; Mn; green; Zn: blue; Cu: purple; Pb: yellow; Cr: pink; Ni: orange) in the bulk and the fine sediments, respectively.

Table 1
Pseudo-total metal (Fe (mg·g^{-1}), Mn, Cu, Cr, Ni, Pb and Zn (μg g^{-1})) content, Enrichment Factor (EF) and Individual Contamination Factor (ICF) were determined in the bulk (<2 mm) and the fine (<63 μm) surface sediments at each sampling site in October 2015. Median and standard deviation (SD) are calculated for each particle size.

		Pseudo-total content													
		Fe		Mn		Cu		Ni		Cr		Pb		Zn	
River	Sites	*Bulk*	*Fine*	*Bulk*	*Fine*	*Bulk*	*Fine*	*Bulk*	*Fine*	*Bulk*	*Fine*	*Bulk*	*Fine*	*Bulk*	*Fine*
Deba	D1	32.9	24.16	419	356	15.5	25.5	26.6	30.5	21.6	36.6	18.6	34.8	170	176
Deba	D2	59.2	30.07	544	491	59.6	100	32.0	35.0	51.5	48.8	12.5	53.2	261	389
Deba	D3	68.2	28.25	972	1177	60.7	70.2	37.4	42.5	28.7	46.5	16.2	29.4	288	421
Deba	D4	68,1	27.22	811	588	58.9	87.8	45.9	53.9	44.0	77.6	26.7	33.1	373	570
Deba	D5	70.8	26.14	902	664	66.1	95.0	46.8	52.8	63.9	78.5	61.8	33.7	407	591
Deba	D6	46.9	37.85	993	1168	51.3	145	68.0	60.4	56.9	88.6	10.3	57.2	406	581
Ego	E1	26.5	22.72	925	442	13.3	44.9	18.5	47.2	33.5	257	13.8	144	148	1087
Ego	E2	34.7	29.77	925	441	69.6	236	38.7	98.7	41.5	318	9.66	101	306	2240
Median		53.1	27.8	914	539	59.3	91.4	38.1	64.5	42.7	78.0	15.0	44.0	297	576
% SD		35.3	16.4	26.3	49.1	45.0	65.2	38.3	40.1	33.8	89.9	81.7	67.4	33.8	33.8

(*) Pb content in residual fraction is below the detection limit, so that ICF was not calculated. (**) Metal speciation at E1 was not determined, so that ICF was not calculated.

Calvo et al., 2017). However, no study has addressed the role of sediment particle size in the mobilization, deposition, and dispersion of potentially toxic metals in the Deba River catchment.

In October 2015, surface sediment samples were collected from six sampling sites along the main river bank (D1, D2, D3, D4, D5 and D6) and from two sampling sites in the Ego tributary (E1 and E2) (Fig. 1). These sampling locations were chosen with a view to studying the influence of natural processes or anthropogenic metal sources on the chemical quality of surface sediments. As per USEPA (2001), surface sediment subsamples (0–5 cm depth) from multiple points within each sampling site were collected using a sterilized plastic spoon, sieved through a 2 mm mesh, composited in the field and sealed in sterile polyethylene bags.

A water sample gathering programme was established to study the involvement of suspended particulate matter (SPM) in metal transport towards the Bay of Biscay. The programme consisted of manual sampling of water in sterile polyethylene bottles monthly or bimonthly from January 2015 to January 2016 at the same six sampling sites along the main river and at three sampling sites in the Oñati (O1) and Ego (E1 and E2) tributaries. In addition, discharge data (Q, m^3 s^{-1}) were monitored daily at the catchment outlet in the Altzola gauging station (www.gipuzkoahidraulikoak.eus/es/deba) to determine different hydrological conditions during the study period. All water and sediment samples were stored and refrigerated in the dark and transported to the Chemical and Environmental Engineering laboratory (University of the Basque Country) on the same day.

2.2. Laboratory methodology

Surface sediments were air-dried and ground with a pestle and mortar for homogenization. The fine fraction of the surface sediments (<63 μm) was sieved through a stainless-steel sieve. The moisture content of all samples was determined in accordance with APHA-AWWA-WPCF, 1999.

2.2.1. Molecular/mineralogical analysis

For molecular characterization of the surface sediment samples, X-ray Diffraction (XRD) and infrared (IR) spectroscopies were used. The XRD analyses were performed using a PANalytical Xpert PRO powder diffractometer equipped with a copper tube (λCuKαmedia = 1.5418 Å, λCuKα1 = 1.54060 Å, λCuKα2 = 1.54439 Å), a vertical goniometer (Bragg−Brentano geometry), a programmable divergence aperture, an automatic interchange of samples, a secondary graphite monochromator, and a PixCel detector. The software PANalytical X'pert HighScore can provide a semiquantitative approximation of the compounds in each sample. The IR laboratory equipment was a Jasco 6300 FTIR spectrophotometer in transmittance mode. All IR spectra obtained in the laboratory were collected in the middle infrared region (from 4000 to 400 cm^{-1}), recording 32 scans per spectrum at a spectral resolution of 4 cm^{-1}.

2.2.2. Elemental analysis

For the elemental spectroscopic analysis, 0.5 g of the fine surface sediment samples was pressed at a pressure of 9 t in a CrushIR (PIKE Technologies, Canada) hydraulic laboratory press; the final pellets had an approximate diameter of 12 mm and an approximate width of 1 mm. For the purposes of creating elemental distribution maps, the <63 μm grain size sediment samples were selected, due to the higher concentration of the study elements in this fraction.

Scanning Electron Microscopy with Energy Dispersive Spectroscopy (SEM-EDS) analyses on fine sediment pellets was used for electron image acquisitions and elemental composition determination using an X-Max energy dispersive X-ray spectrometer (Oxford Instruments, Abingdon, Oxfordshire, U.K.) coupled to an EVO40 scanning electron microscope (Carl Zeiss NTS GmbH, Germany). SEM images were acquired at high vacuum, employing an acceleration voltage of 20 kV. Magnifications up to 10,000× were achieved using a secondary electron (SE) detector. The elemental analysis was carried out using a working distance of 8.5 mm, take-off angle of 35°, and an acceleration voltage of 30 kV. An integration time of 50 s was used to improve the signal-to-noise ratio of EDS spectra. Spectral data were processed using INCA software (Oxford Instruments, Abingdon, Oxfordshire, U.K.). This software can provide a semiquantitative approximation of the elements contained in the surface sediment samples under study, based on the K-alpha net areas of each element detected. Additional information relating to the instrument, measurement conditions, and spectral assignment can be reviewed elsewhere (Aramendia et al., 2018; Gómez-Nubla et al., 2013).

2.2.3. Pseudo total and sequential metal extraction

The pseudo total metal content was measured using an ETHOS 1, Millestone microwave digestion system, where three replicates of each surface sediment sample (0.5 g) were heated in Teflon vessels with concentrated HNO_3:HClO (3:1.5) by raising the temperature to 180 °C for 10 min and maintaining this level for an additional 25 min (USEPA, 2007).

The metal distribution was determined by sequential extraction of metals using the procedure developed by the European Community Bureau of References (BCR 701), which is divided into four operationally-defined fractions: (i) exchangeable and acid-extractable (F_1, soluble species, carbonates and exchangeable metals), (ii) reducible (F_2, Fe/Mn oxyhydroxides), (iii) oxidizable (F_3, organic matter and sulphides), and (iv) residual fraction (F_4, remaining non-silicate bound metals).

The metals under consideration (Fe, Mn, Zn, Cu, Ni, Cr and Pb) in the sequential extracts and pseudo-total digestion were determined by ICP-OES (Perkin Elmer Optima 2000). The detection limit for these metals was: Pb (1 μg g^{-1}), Mn (0.5 μg g^{-1}), Fe and Mn (0.4 μg g^{-1}) and Cr,

EF												ICF													
Mn		Cu		Ni		Cr		Pb		Zn		Fe		Mn		Cu		Ni		Cr		Pb		Zn	
Bulk	*Fine*	*Bulk*	*Fine*	*Bulk*	*Fine*	*Bulk*	*Fine*	*Bulk*	*Fine*	*Bulk*	*Fine*	*Bulk*	*Fine*	*Bulk*	*Fine*	*Bulk*	*Fine*	*Bulk*	*Fine*	*Bulk*	*Fine*	*Bulk*	*Fine*	*Bulk*	*Fine*
0.75	0.86	1.02	2.28	1.34	2.10	0.58	1.34	1.03	2.62	3.07	4.33	0.10	0.37	6.63	7.99	0.35	1.54	1.40	1.80	0.23	0.09	3.89	(*)	0.38	1.55
0.54	0.96	2.18	7.20	0.90	1.93	0.77	1.43	0.38	3.22	2.61	7.70	0.04	0.32	0.96	6.24	0.74	4.59	0.30	1.55	0.19	0.22	2.50	(*)	0.74	4.24
0.84	2.44	1.92	5.37	0.91	2.50	0.37	1.45	0.43	1.89	2.51	8.85	0.02	0.45	1.74	16.5	0.30	4.31	0.35	2.19	0.11	0.24	0.32	(*)	0.10	5.75
0.70	1.27	1.87	6.97	1.12	3.29	0.57	2.52	0.71	2.21	3.25	12.4	0.03	0.28	0.82	6.10	0.74	4.34	0.67	2.39	0.87	1.06	1.90	(*)	0.92	7.76
0.75	1.49	2.02	7.85	1.10	3.36	0.80	2.65	1.59	2.35	3.42	13.4	0.02	0.23	0.74	7.27	0.22	4.97	0.26	2.39	0.36	1.03	0.60	(*)	0.68	8.55
1.24	1.81	2.36	8.27	2.41	2.65	1.07	2.07	0.40	2.74	5.15	9.12	0.03	0.31	0.69	7.74	0.37	8.13	0.26	2.56	0.16	0.83	0.97	(*)	0.86	7.57
2.05	1.14	1.08	4.27	1.16	3.45	1.12	9.98	0.95	11.5	3.32	28.4	(**)													
1.56	0.87	4.33	17.1	1.85	5.51	1.06	9.44	0.51	6.16	5.23	44.7	0.05	0.24	0.30	4.46	0.79	4.74	0.10	2.48	0.32	1.89	3.14	28.6	1.77	9.48
1.05	1.35	2.10	7.41	1.35	3.10	0.80	3.86	0.75	4.09	3.57	16.1	0.04	0.31	1.69	8.04	0.50	4.66	0.48	2.20	0.32	0.77	1.90	28.6	0.91	6.41
49.6	40.4	48.8	59.3	38.9	36.5	34.6	94.5	56.2	80.4	29.4	84.5	66.5	24.4	131	48.7	48.4	41.2	93.0	17.3	80.8	83.7	70.7		47.4	43.2

Cu and Ni (0.1 μg g^{-1}). Additionally, the recovery percentage for each metal in each step of sequential extraction was calculated taking into account pseudo-total digestion. For all elements, it stood in a range of 94% to 119%.

For the purposes of controlling analytical methods, a NBS sediment sample was also used (Buffalo River sediment, USA). Using this technique, all metals were also measured with mean values close to the certified contents and variation coefficients lower than 8%, except for Pb (17% with 0.5 g of sample).

Water samples collected at all sampling locations were filtered through 0.45 μm filters and the residue was oven-dried at 105° for 1 h. The concentration of the SPM was obtained from the weight of each dried residue and the volume of the sample. The pseudo-total metal (Fe, Mn, Zn, Ni, Cu, Cr and Pb) contents in the SPM were determined using the acid-digestion methodology described above for surface sediments.

2.3. Assessment of chemical quality of surface sediments

Based on the work of Skeries et al. (2017), it was decided to use the Divergence Factor (DF) in this study to identify how far a sampling location deviated from the dominant trend in the Deba River catchment in terms of pseudo-total content of the metals in surface sediments. Firstly, the pseudo-content of each element from each sampling site [M] was divided by its respective median value throughout the catchment (Eq. (1)). Thus, metal content in surface sediments was considered anomalous when normalized concentration exceeded 1. The median-normalized values for the metals of interest were then totalled for each sampling site (Eq. (2)).

$$\text{Normalized concentration} = \frac{[M]}{\text{Median } [M]} \tag{1}$$

$$DF = \sum_{i=1}^{n=7} \text{Normalized concentration} \tag{2}$$

Enrichment of a given element in sediments relative to a background reference site is an indication of the contribution from nature (e.g. weathering process of rocks) and anthropogenic sources (Violintzis et al., 2009; Legorburu et al., 2013; Gu et al., 2015). The Enrichment Factor (EF) for each metal was calculated in accordance with Eq. (3), where $[M]_S$ and $[R]_S$ are the concentrations of the metal M and the reference element R in surface sediment samples, while $[M]_{rf}$ and $[R]_{rf}$ are the concentrations in the upper continental crust (Delshab et al., 2017). The use of local non-polluted sediments as the background reference instead of the crust has been widely proposed in order to deal with the geochemical heterogeneity in nature (Reimann and De Caritat, 2005; Dung et al., 2013; Mali et al., 2015). However, we declined to establish the headwater locations (D1 and E1) as the reference due to the unexpectedly high concentrations of some metals with respect to the region as a whole (Table 1). Given that the surface sediments from the Deba River catchment were rich in Fe content and that Fe was strongly retained in the lattice of mineral in both bulk (<2 mm) and fine (<63 μm) fractions (as shown below), it was considered to be mainly a lithogenic component, and thus an appropriate reference element for EF calculation. Jiao et al. (2015) propose a six-category system to describe the contamination level. EF < 1, no enrichment; 1 ≤ EF < 2, deficiency to minimal enrichment; 2 ≤ EF < 5, moderate enrichment; 5 ≤ EF < 20, significant enrichment; 20 ≤ EF < 40, very high enrichment; and EF ≥ 40, extremely high enrichment. The global enrichment factor (GEF) is equal to the sum of the enrichment factor of all metals at each sampling site (Eq. (4)).

$$EF = \frac{([M]_S/[R]_S)}{([M]_{rf}/[R]_{rf})} \tag{3}$$

$$GEF = \sum_{n=1}^{n=6} EF \tag{4}$$

Determination of Individual and Global Contamination Factors of metals (ICF and GCF, respectively) is an important tool for indicating the degree of risk of metal contamination to the environment in relation to retention time in sediments (Naji et al., 2010; Saleem et al., 2015). ICFs were obtained for each metal from the results of the fractionation study, dividing the sum of the concentrations (C) in the first three extractions (F_1, F_2 and F_3, constituting the non-residual fraction) by that in the residual fraction (F_4) at each sampling site (Eq. (5)). The GCF is equal to the sum of individual factors (Ikem et al., 2003; Naji et al., 2010), as shown in Eq. (6).

$$ICF = \frac{\text{C non}-\text{residual}}{\text{C residual}} \tag{5}$$

$$GCF = \sum_{i=1}^{n=7} ICF_i \tag{6}$$

2.4. Statistical analysis

Once a Shapiro Wilk test confirmed that variables were not normally distributed, all data were log-transformed in order to reduce the skewness of the data.

A Spearman correlation analysis (non-parametric test) was performed with metal pseudo-contents to establish the relationships between the bulk and the fine surface sediments. In addition, the effect of variability of composition and properties between particle sizes on the availability of metals in surface sediments was analysed using one-way ANOVA (taking $\rho < 0.05$ as significant, in accordance with

Tukey's multiple range test). The variability of metal pseudo-contents in SPM during different hydrological conditions was also analysed to evaluate the influence of seasonality on sediment dynamics. In addition, the predominance of two physical mechanisms involved in metal dispersion were evaluated using regression analysis between surface sediments and SPM. Finally, principal component analysis (PCA) was used to identify the natural process or anthropogenic activity representing the main source of available metals in surface sediments at each sampling site. PCA with an eigenvalue of over 1 was subjected to an orthogonal varimax rotation. This maximises the variance to obtain a pattern of loadings for each factor that is as diverse as possible, thus making it easier to interpret. Statistical processing of the data was performed using SPSS 22.0 software.

3. Results and discussion

3.1. Mineralogical and elemental characterization of surface sediments

XRD analyses were performed for molecular and mineralogical characterization of the surface sediment samples. The diffractograms (see for example Fig. S1) showed quartz (SiO_2), calcite ($CaCO_3$, except in D1), illite ($K_{0.65}Al_{2.0}[Al_{0.65}Si_{3.35}O_{10}](OH)_2$), and clinochlore ($Mg_5Al(AlSi_3O_{10})(OH)_8$) in all samples and both grain sizes. Albite ($NaAlSi_3O_8$) was observed particularly at D6 (<63 μm). Oxides and hydroxides of iron (hematite, Fe_2O_3 and goethite, FeO(OH)) were found as trace, except in the case of E2 (<2 mm) for hematite.

As an estimation of the relative proportion of the identified minerals, the semiquantitative results (Fig. 2) showed that all fine (<63 μm) surface sediments, except D1 and E1 had the following mineralogical composition order: Illite > Quartz > Calcite > Clinochlore. In contrast, the compositional sequence of bulk (<2 mm) surface sediments varied throughout the catchment, suggesting that the bulk fraction better integrates and explains the differences in the mineralogical composition of the study area, whereas the fine fraction is useful for evaluating the extent and influence of weathering on the maturity of surface sediments. The term maturity refers to the cumulative changes undergone by sedimentary particles during erosion, weathering, and transport until their final deposition as sediments (Warrier et al., 2016).

Thus, given that carbonate minerals have higher solubility than silicate minerals (Szramek et al., 2011) and smaller particles have a larger surface area in contact with water, we expected to find lower percentages of unstable ones (e.g. calcite) in the fine surface sediments than in the bulk surface sediments. In effect, the higher the particle-size, the greater the proportion of quartz (except at D2 and E2), clinochlore (except at D1 and E1) and, primarily, calcite. Conversely, the percentage of illite, a clay mineral and one of the products of feldspar dissolution (Ma et al., 2017), was higher in the fine surface sediments. In addition, the presence of carbonate minerals in the bulk mineral analysis of the loess/palaeosol sequence was used by Terhorst et al. (2012) to classify the weathering intensity at the lower degree. Based on that classification, surface sediments from the Deba catchment would be considered to be in the earliest stages of maturity. Indeed, water erosion is the dominant geomorphological force ahead of karstification in calcareous sites, due to the high rainfall and orographic features of the region (URA, 2004).

Focusing on the bulk fraction, the spatial distribution of the mineralogy concurs with the lithological characteristics of each sub-basin (Fig. 2). The headwater of the main channel (D1) was characterized by high proportions of illite and quartz, and the absence of calcite, due to the predominance of sandstones/mudstones and the limited occurrence of limestones in the area. D2-D3 and D4-D5 presented similar lithology and, therefore, mineralogy. In contrast to D1, an increase in the occurrence of limestones and marls, especially at D4 and D5 (Fig. 2), encouraged higher calcite proportions downstream. The highest percentages of quartz were observed upstream of the Ego tributary (E1) due to the predominance of sandstones/mudstones, while downstream (E2) calcite was the principal mineral. The fact that carbonate rocks are not characteristic of the lithology at E2 suggests that this mineral was transported from the Aixola watershed (Fig. 1A), where most of the main bedrock consists of practically impervious Upper Cretaceous Calcareous Flysch (Meaurio et al., 2015). Finally, despite the fact that limestones predominate in the lithology, the outlet of the catchment (D6) presented similar percentages of all minerals. This could be attributed to the confluence of the Deba River with the Ego tributary, which considerably increases the river discharge. Hence, a greater discharge explains extensive transport of silicate minerals caused by water erosion of the sandstones/mudstones that form the bedrock from immediately upstream (Altzola gauging station subbasin, Fig. 1A).

In accordance with the XRD results, the mid-infrared (MIR) spectra (Fig. S2) identified O—H stretching of free and bound hydroxyl groups

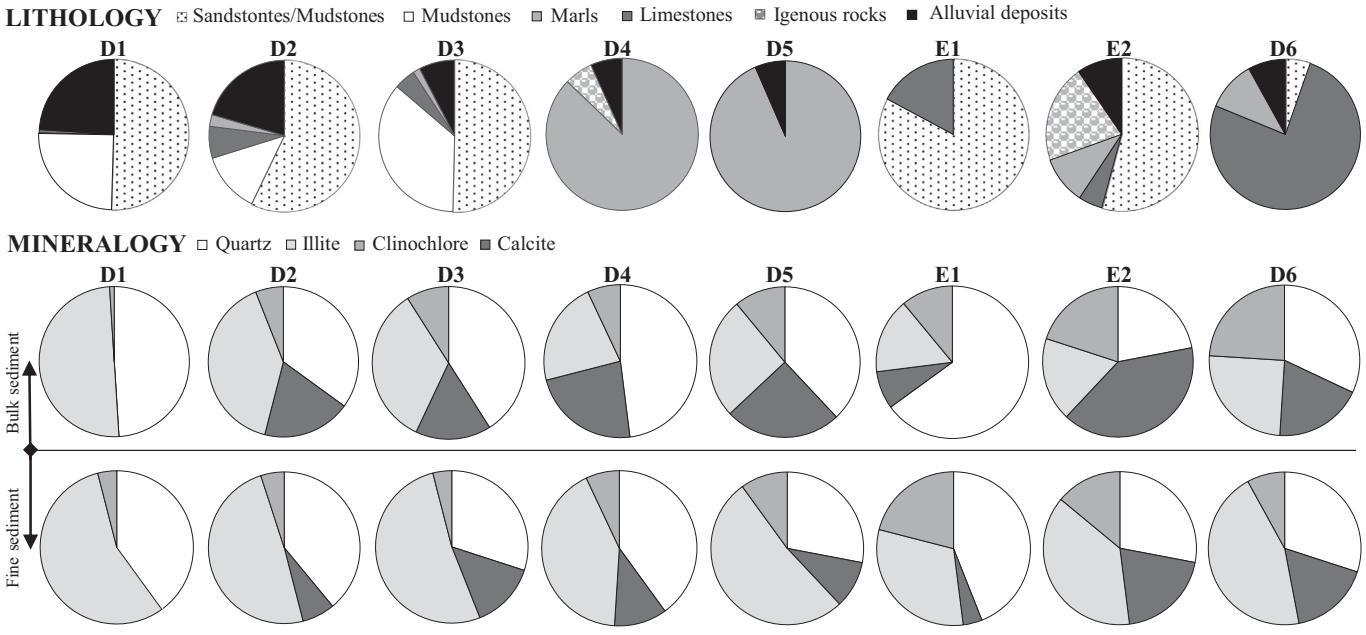

Fig. 2. Lithology of the sub-basins where sampling sites are located and percentage mineralogical distribution of the bulk and fine sediment samples using XRD.

(at 3628 cm^{-1}), suggesting the presence of clay minerals. The detected Si—O—Si and Si—O stretching vibrations (at 1000 and 694 cm^{-1}, respectively) may be related with silicate minerals —principally illite and kaolinite—, while quartz double peaks are observed at 776 and 795 cm^{-1}. Finally, the bands located at 1420, 872 and 712 cm^{-1} are associated with the presence of calcium carbonate, and weak peaks at around 796 cm^{-1}, 745 cm^{-1} and 725 cm^{-1} could be attributed to other carbonated elements (e.g. Mg^{2+}, Li^{+}, K^{+} and Na^{+}) (Song et al., 2012). Moreover, the curvature found at 912 cm^{-1} may be characteristic of Al-OH stretching vibration due to the presence of $Al(OH)_3$ or even hematite.

Broad bands corresponding to C—H (from 200 to 3100 cm^{-1}) and C═O (at 1797 cm^{-1}) are likely to be characteristic stretching vibrations of aliphatic hydrocarbons, and aldehyde, ketone, ester or carboxylic acid, respectively. On the other hand, the band at 1636 cm^{-1} corresponds to C═C and C═O characteristics stretching vibration of organic matter. As for spatial distribution, it should be highlighted that both particle sizes of surface sediments presented higher areas of these bands downstream of all the WWTPs (D3, D5 and D6).

For elemental characterization of the fine surface sediment samples, we selected different areas on each pellet where Fe, Mn, Cu, Ni, Cr, or Zn had previously been identified in several EDS spectra.

Firstly, the omnipresence of illite in the fine surface sediments (Fig. 2) was corroborated since the similarity among K, Al and Si maps implied the formation of potassium aluminium silicates (Fig. S3A). Mg also appeared with Al and Si, indicating the presence of magnesium aluminate or magnesium alumina-silicate as clinochlore (Fig. S3B). On the other hand, no correlation among Ti, Ca, Fe and Mg maps (Fig. S3A) suggested the presence of oxides such as rutile or anatase (TiO_2), hematite (Fe_2O_3) or goethite (FeOOH).

Finally, a high correlation of Fe with Al and Si, and with K^{+}, Na^{+} or Mg^{2+} highlighted that it was preferentially retained in the mineral lattice of fine surface sediments. Alternatively, the distribution maps of Zn, Cu, Ni, and Cr showed no correlation with other elements except O and C. This might indicate that they were presented mainly as oxide or hydroxide or bound to the organic matter, except at D6 and E2 where Cu and Zn, respectively, were correlated with sulphur, suggesting that they were presented as sulphate or sulphide.

3.2. Pseudo total and sequential metal extraction in surface sediments

As shown in Table 1, median pseudo-contents of metals (Fe, Mn, Zn, Ni, Cu, Cr and Pb) in the fine surface sediments were higher than in the bulk surface sediments, except for Fe and Mn. These results concur with those of other authors who showed that concentrations of metals tend to increase with a decrease in particle grain size (Zhang et al., 2002; Morelli et al., 2012; Yao et al., 2016; Kang et al., 2017). The fine fraction is the most chemically active sediment phase due to its high capacity for cationic exchange, resulting from a high content of secondary minerals (e.g. clay minerals, Fe and Mn oxides and hydroxides, and carbonates) and organic matter (Hardy and Cornu, 2006), and the large surface area per unit mass, which gives it greater adsorption capacity (Guven and Akinci, 2013). Indeed, the bulk fraction had a higher content of quartz, which gives it a very weak adsorption capacity at a particle size of <2 mm (Horowitz, 1991). Additionally, as observed in EDS spectra of the fine sediments from almost all sampling sites (Fig. S3B), Fe and Mn appeared together, suggesting the presence of Fe/Mn oxyhydroxides. However, high quantities of Fe oxides might also be found in the coarse fraction (Devesa-Rey et al., 2011), such as hematite (Fe_2O_3) in the bulk surface sediments from E2. Thus, coatings, probably formed by Fe and Mn oxides on the sandy fraction might explain the predominance of these metals in the bulk surface sediments.

Reflecting the influence of particle size on the adsorption capacity of surface sediments, the metal concentration in the two fractions is not correlated ($\rho < 0.5$) and two different content patterns could be identified: Fe > Mn > Zn > Cu > Cr > Ni > Pb and Fe > Zn > Mn > Cr > Cu > Pb > Ni, for the bulk and fine fractions, respectively (Table 1). Otherwise, Ni significantly correlates with Zn ($\rho = 0.976$ at 0.01 level), and in general, positive correlations between Zn, Ni and Cr were found in the bulk fraction. Similarly, these metals are highly correlated in the fine surface sediments, suggesting that they had the same origin. However, correlations between Fe—Cu, Ni—Cu and Pb—Cr ($\rho > 0.714$ at 0.05 level) in the fine fraction imply different possible metal sources.

The textures of surface sediments from the Deba River catchment display a predominance of the sandy fraction (0.063–2 mm), with percentages of over 91%. The proportion of heavy metal loading from the fine (<63 μm) to the bulk fraction (<2 mm) was calculated from the metal content and the mass percentage of the fine sediment fraction. Only approximately 3.0–14.5 (%) of the total metal loading (unpublished data) was retained in the <63 μm fraction, conclusively demonstrating the importance of analysing both particle sizes to provide a more reliable reflection of the risk associated with metals in surface sediments.

As for spatial distribution, the lowest pseudo-contents in the main channel were measured upstream at D1 for all metals, except for Pb (Table 1). In contrast, the headwater of the Ego tributary (E1) presented a deviation of over 30% with respect to D1 for Mn, Ni and Cr in the bulk surface sediments, and Zn, Ni, Cu, Pb and Cr in the fine surface sediments, supporting the idea that sampling sites considered as non-disturbed (Fig. 2) had a different lithological composition.

By determining the Divergence Factor (DF), it is possible to identify the sampling locations that are most anomalous with respect to the region as a whole, with regard to metal pseudo-content in surface sediments. When the bulk fraction is considered, D4, D5 and D6 are of concern (Fig. 3A). Indeed, D5 and D6 had the highest concentrations of Fe-Cr-Pb and Mn—Ni, respectively (Table 1). However, the maximum values for Pb, and for Cu, Ni, Cr and Zn were found in the fine surface sediments up- (E1) and downstream of the municipalities of Ermua and Eibar (E2) respectively. Consequently, the Ego tributary, and the mid-part and the outlet of the Deba River are a priori the most potentially contaminated areas of the catchment. Indeed, normalized concentrations >1 of all metals mainly at mid- (D4 and D5) and downstream (E2 and D6) sampling sites (Fig. 1B) suggest the existence of significant metal inputs in these locations.

Table 1 clearly shows that anthropogenic influence increases, to a greater (Pb and Cr) or a lesser (Mn and Ni) extent, from the bulk to the fine fraction. In the case of the bulk surface sediments, only the median EF values for Cu and Zn show moderate anthropogenic pollution. However, metal pseudo-contents in the fine surface sediments represent a moderate (Pb, Cr and Ni) or even significant (Zn and Cu) enrichment. The extreme anthropogenic pollution at E1, due primarily to Zn and Pb (Table 1), should be noted. This contradicts the premise that the headwater of the Ego tributary is a non-disturbed area. Vehicle emissions from the main national road and motorway (Fig. 1B) might be the main source of these metals in surface sediments (Saeedi et al., 2009; Adamiec et al., 2016). It is also interesting to note the strong relationship between DF and GEF for the fine fraction (Fig. 3A), which suggests that anthropogenic sources of metals are responsible for the anomalies throughout the catchment, especially in the Ego tributary (E1 and E2), and mid- (D5) and downstream (D6) of the main river. In the case of the bulk fraction, the absence of a linear relation between factors (Fig. 3A) indicates that anomalies are fundamentally due to metal contribution from nature sources.

The results of sequential extraction of metals (Fe, Mn, Zn, Cu, Ni, Pb and Cr) in the bulk and fine surface sediments are shown in Table 2. The concentration of all metals in the three mobile fractions (F_1, F_2 and F_3) significantly increased ($\rho < 0.05$) with decreasing grain size, except for Fe and Cr in the exchangeable and acid-extractable fraction (F_1), and for Mn, Zn, Ni and Cr in the oxidizable fraction (F_3). In contrast, the proportion of all metals in the residual fraction (F_4) significantly decreased ($\rho < 0.05$) with decreasing grain size, except for Cr. The higher percentages of the mobile fractions in the <63 μm particle size suggest a

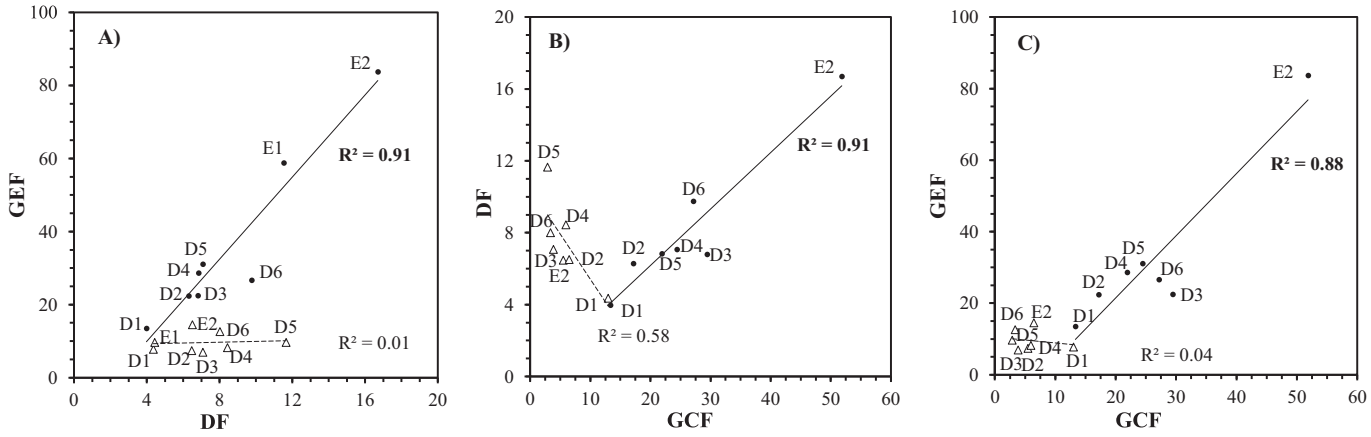

Fig. 3. Linear relationships between Divergence Factor (DF), Global Enrichment Factor (GEF) and Global Contamination Factor (GCF) taking all sampling sites into consideration (except E1 in graphics B and C) for the bulk (<2 mm; triangles) and the fine (<63 μm; circles) surface sediments.

preference of the available metals —mainly attributed to an anthropogenic input (Ramirez et al., 2005; Tiquio et al., 2017)— for smaller particles. Meanwhile, the predominance of the residual fraction in the <2 mm grain size indicates that metals were strongly retained in the mineral lattice and, consequently, that they were largely contributed by lithogenic sources (Kang et al., 2017).

The mean ICF (Table 1) of metals are ranged in the order Pb > Mn > Zn > Cu > Ni > Cr > Fe, with no variation between particle sizes. Considering that ICF reflects the risk to a water-sediment body of a pollutant, the bulk surface sediments only represented a risk (ICF > 1) from Mn and Pb, especially at D1. Conversely, all metals in the fine surface sediments were widely available in all sampling sites, mainly at E2, D3 and D6. The strong positive relationships between GCF and DF (Fig. 3B), and GCF and GEF (Fig. 3C) for the fine surface sediments indicate that anomalies found throughout the catchment were due to the most mobile metals, which were likely to come from anthropogenic sources. Conversely, the negative relationship between GCF and DF (Fig. 3B) for the bulk surface sediments suggests that metals in the residual fraction (F_4) and, consequently, lithological characteristics of each sub-basin were responsible for the anomalies.

In order to obviate the greater abundance of metals in the residual fraction of the bulk surface sediments than in the fine surface sediments, and to identify different metal partitioning in the entirely non-residual fraction (F_{123}) depending on particle size, the results for the mobile fractions were recalculated (unpublished data) based on their sum ($F_1' = F_1/F_{123}$; $F_2' = F_2/F_{123}$; and $F_3' = F_3/F_{123}$, respectively). Two metal behaviours were distinguished:

(a) The chemical distribution of Mn and Cr did not vary between grain sizes and the results are consistent with the study by Kang et al. (2017). The greatest proportion of Mn was mainly associated with F_1' (44.9–55.4%), followed by reducible (F_2') and oxidizable (F_3') fractions (31.7–37.3% and 7.32–23.5%, respectively). Although sensitive to reducing conditions, the relative predominance of Mn in the exchangeable fraction was due to compounds of this element being solubilized in surface sediments submitted to continuous changes in their redox state (Devesa-Rey et al., 2010). The highest proportion of Cr was mainly associated with F_3' (74.3–94.3%), followed by F_2' and F_1' (4.09–24.1% and 1.65–1.71%, respectively). The widespread presence of Cr in the oxidizable fraction might be related to the fact that in oxidation state, this metal could be associated with organics or adsorbed in hydrous form onto sediments (Filipek and Owen, 1979).

(b) The chemical distribution of Fe, Pb, Cu, Ni and Zn varied between sediment fractions, with the influence of the different composition and properties of particle sizes particularly noticeable on the behaviour of metals in the water environment (Yao et al., 2016). The oxidizable fraction (F_3') was the most abundant non-lithogenous fraction (57.5–93.2%) for Cu in both grain sizes. Its high affinity to humic substances (Davutluoglu et al., 2011)

Table 2
Metal distribution in the bulk (<2 mm) and the fine (<63 μm) surface sediments for all sampling sites ($N = 7$). The mean and standard deviation (±SD) data are presented in μg g^{-1} for all metals, except for Fe (mg g^{-1}). The value in parentheses show percentage of elemental concentration, where the highest percentage for each metal is shown in bold. Sum: $F_1 + F_2 + F_3 + F_4$; the Total was determined by microwave assisted acid digestion; Recovery (%): (Sum/Total) × 100.

	F_1 Exch./Carbonates	F_2 Reducible	F_3 Oxidizable/Sulphides	F_4 Residual	Sum	Total	Recovery
Bulk							
Fe	0.057 ± 0.036 (0.106)	0.798 ± 0.315 (1.48)	0.970 ± 0.395 (1.80)	52.1 ± 15.7 (**96.6**)	53.9	54.2	99
Mn	175 ± 98.2 (22.1)	117 ± 52.8 (14.7)	83.4 ± 39.5 (10.5)	417 ± 205 (**52.6**)	793	795	100
Zn	56.0 ± 40.1 (16.53)	49.0 ± 34.4 (14.5)	58.0 ± 23.9 (17.1)	176 ± 33.7 (**51.9**)	339	315	108
Ni	3.99 ± 1.57 (9.83)	3.67 ± 2.72 (9.05)	2.91 ± 2.45 (7.17)	30.0 ± 12.9 (**74.0**)	40.6	42.0	97
Cu	1.00 ± 1.08 (1.62)	0.386 ± 0.616 (0.623)	18.8 ± 10.0 (30.3)	41.8 ± 15.5 (**67.5**)	62.0	55.5	112
Pb	0.181 ± 0.141 (0.844)	1.84 ± 1.59 (8.59)	9.20 ± 4.15 (43.0)	10.2 ± 9.04 (**47.6**)	21.4	22.0	97
Cr	0.243 ± 0.359 (0.531)	0.433 ± 0.540 (0.943)	10.3 ± 8.20 (22.5)	34.9 ± 15.1 (**76.1**)	45.9	43.8	105
Fine							
Fe	0.030 ± 0.024 (0.104)	4.36 ± 1.08 (15.1)	2.41 ± 0.786 (8.36)	22.0 ± 3.59 (**76.4**)	28.8	29.1	99
Mn	405 ± 229 (**48.9**)	290 ± 209 (35.0)	40.7 ± 21.7 (4.91)	92.4 ± 37.5 (11.2)	828	698	119
Zn	219 ± 263 (32.6)	299 ± 320 (**44.6**)	74.2 ± 74.5 (11.1)	78.9 ± 60.14 (11.8)	670	710	94
Ni	13.7 ± 6.39 (23.2)	18.8 ± 7.05 (**31.8**)	8.44 ± 4.17 (14.3)	18.1 ± 5.49 (30.7)	59.0	53.4	110
Cu	9.82 ± 16.6 (9.43)	35.0 ± 30.0.7 (33.6)	41.6 ± 17.8 (**39.9**)	17.8 ± 10.6 (17.1)	104	108.4	96
Pb	2.27 ± 1.65 (4.03)	38.6 ± 12.4 (**68.5**)	15.0 ± 13.6 (26.6)	0.487 ± 1.29 (0.864)	56.4	48.9	115
Cr	1.48 ± 3.02 (1.42)	11.1 ± 12.8 (10.6)	40.0 ± 55.9 (38.3)	51.7 ± 27.1 (**49.6**)	104	99.2	105

favours a pronounced tendency for complexation with sediment organic matter. However, the predominance of the reducible fraction (F_2') over the exchangeable fraction (F_1') in the fine surface sediments might be related to the higher content of Fe/Mn oxides and hydroxides (F_2; Table 2). The prevalence of Fe in the reducible fraction of the fine surface sediments (F_2'; 64.25%) also appears to influence the partitioning of Zn, Ni and Pb in the smallest particle size. Pb bound to F_2' (71.2%) exceeds Pb bound to F_3' (25.0%) in the fine surface sediments, despite the tendency of lead to form stable organic complexes and/or to be bound to sulphides (Tüzen, 2003). Although Ni and Zn were distributed between three mobile fractions in both grain sizes, they were also mainly bound to F_2' (46.9%) in the fine surface sediments.

Regardless of chemical distribution changes in F_{123}' between the bulk and the fine surface sediments, it was observed that the reducible (F_2') and the oxidizable (F_3') were the fractions which showed significant differences between particle sizes ($\rho < 0.038$) for all metals, except for Ni. In addition, although fine sediments have greater particulate organic carbon (Strom et al., 2011), Fe/Mn oxyhydroxides appeared to be chiefly responsible for the increased adsorption of metals on fine surface sediments to the detriment of organic matter.

Finally, PCAs were performed on the metal percentages in the mobile fraction (F_{123}) to elucidate the main sources of available metals in the bulk and fine surface sediments from the Deba River catchment. The two sets of results were plotted together in Fig. 4 to establish similarities/dissimilarities between grain sizes. PCA produced two principal components, representing 75.3% (PCI: 46.1%; PCII 29.3%) and 71.4% (PCI: 36.2%; PCII: 35.2%) of the total variance for the bulk and the fine fraction, respectively.

Based on the variable loading and sample score, similar clustering of sampling sites could be observed for both particle sizes. However, while the mobile fraction of metals shows a widespread spatial distribution in the bulk surface sediments (from 24.1% to 62.6% of deviation between sampling sites, Fig. S4A), it remains unchanged along the catchment in the fine surface sediments (from 1.3% to 18.2% of deviation, Fig. S4B), hindering the identification of metal sources. Thus, as with the mineralogical analysis, the <2 mm sediment grain size is more useful for identifying different natural or anthropogenic sources of available metals in the study area, while they are masked by the higher influence of downstream transport of the fine surface sediments, as discussed in the section below.

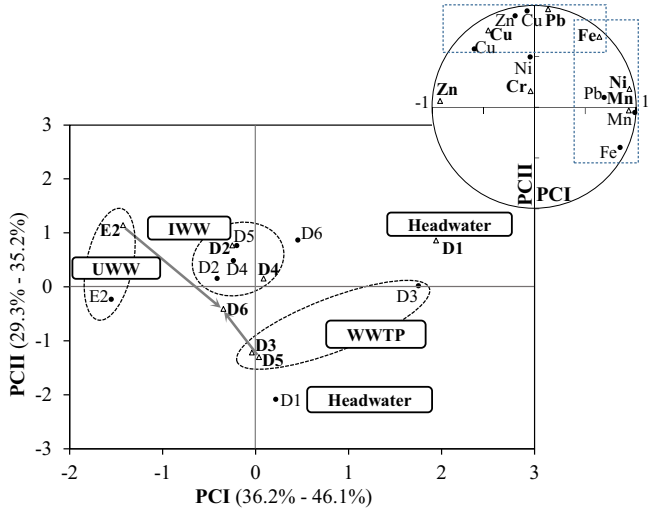

Fig. 4. Principal Components Analysis applied to the mobile fraction (F_{123}) of all metals in surface sediments for all sampling sites (except for E1) and for both grain sizes (<2 mm: triangles; <63 μm: circles).

Unlike the fine fraction, the bulk surface sediments from the headwater of the Deba River (D1) were characterized by having the highest available Fe, Mn, Ni and Pb percentages (8.98%, 86.9%, 58.3% and 79.6% respectively; Fig. S4A). Their maximum percentages in the reducible fraction at D1 (Fig. S4A) and the absence of human activities in this area suggest that these available metals resulted primarily from natural weathering of minerals and their subsequent adsorption into the coatings formed by Fe and Mn oxides on the sandy fraction.

In contrast, industrial wastewaters (IWW) were the main sources of non-lithogenous Cr in the bulk and the fine surface sediments, especially at D4 (46.6%; Fig. S4A and 51.4%; Fig. S4B, respectively). They also provided available Cu (42.6%), Zn (42.5%; mainly at D2), and Pb and Ni (65.5% and 40.1%, respectively; mainly at D4) to the bulk surface sediments. Before connection to the Apraitz WWTP in June 2014, untreated wastewater (UWW) from Ermua appear to have contributed to the fact that the highest percentages of available Zn and Cu (63.9% and 44–0%, respectively; Fig. S4A) were found in the bulk surface sediments, and Cr (65.4%, Fig. S4B) in the fine surface sediments from the Ego tributary (E2). Although residential waste is the chief source of copper in river sediments (Zhai et al., 2003; Paramasivam et al., 2015; Yao et al., 2016), vehicles have been also reported to be one of the contributors to Zn and Cu entering the surface water system, as a result of the combustion of motor fuel, wear on brake linings, tyre wear and car washing (Legret and Pagotto, 1999; Sörme and Lagerkvist, 2002; Rule et al., 2006). Moreover, urban wastewaters are gathered from homes, commercial establishments, industries and storm-water runoff from roads, which are all also likely to be sources of metals.

Otherwise, although effluents from WWTPs are not one of the major pathways of available metals to the bulk surface sediments, Epele WWTP (D3) appears to contribute non-lithogenous Mn (63.5%), Zn (50.0%) and Ni (25.8%). In the case of the fine surface sediments, it contributes to highly mobile Fe (31.0%), Mn (94.3%), Zn (85.2%) and Ni (68.7%). Meanwhile, the Mekolalde WWTP (D5) is grouped together with IWW due to the higher available Cr, probably from D4. WWTPs treat not only urban but also industrial wastewaters, whose dissolved Zn, Ni and Mn has the lowest removal efficiency in the activated sludge process (Yamagata et al., 2010; Ong et al., 2010; da Silva Oliveira et al., 2007). Finally, while available metals in the bulk fraction at D6 came from the Ego tributary (Fe, Zn, Cu and Pb) and upstream (D5; Mn and Zn), one possible anthropogenic source of non-lithogenous Fe, Mn, Ni and Cu in the fine fraction should be noted (the Apraitz WWTP or IWW).

3.3. Transport of contaminants by SPM

The median discharge (Q) value obtained for the 9 sampling campaigns was 10 $m^3\ s^{-1}$. This allows us to establish two different sets of hydrological conditions: a wet season corresponding to sampling months with Q values of over 10 $m^3\ s^{-1}$ (January, February and March 2015, and January 2016); and a dry season comprising months with Q values of below 10 $m^3\ s^{-1}$. Fig. 5 summarizes the SPM content in the water samples and the concentrations of Fe, Mn, Zn, Ni, Cu, Cr and Pb in the SPM in the dry and wet season. Metal content in the SPM shows significantly higher median values during the dry season than during the wet season ($\rho < 0.05$), while the SPM concentration in water samples displayed the opposite behaviour. Indeed, a decrease in water discharge causes less erosion, and thus reduces the transport capacity of the river (Pascaud et al., 2015). However, during low discharge events, resuspended particles tend to be smaller (Palleiro et al., 2013), having high metal concentrations as we observed above for surface sediments.

For a more accurate evaluation of sediment dynamics during the two different hydrological conditions, linear regressions were applied using metals as chemical connectors between SPM and surface sediments

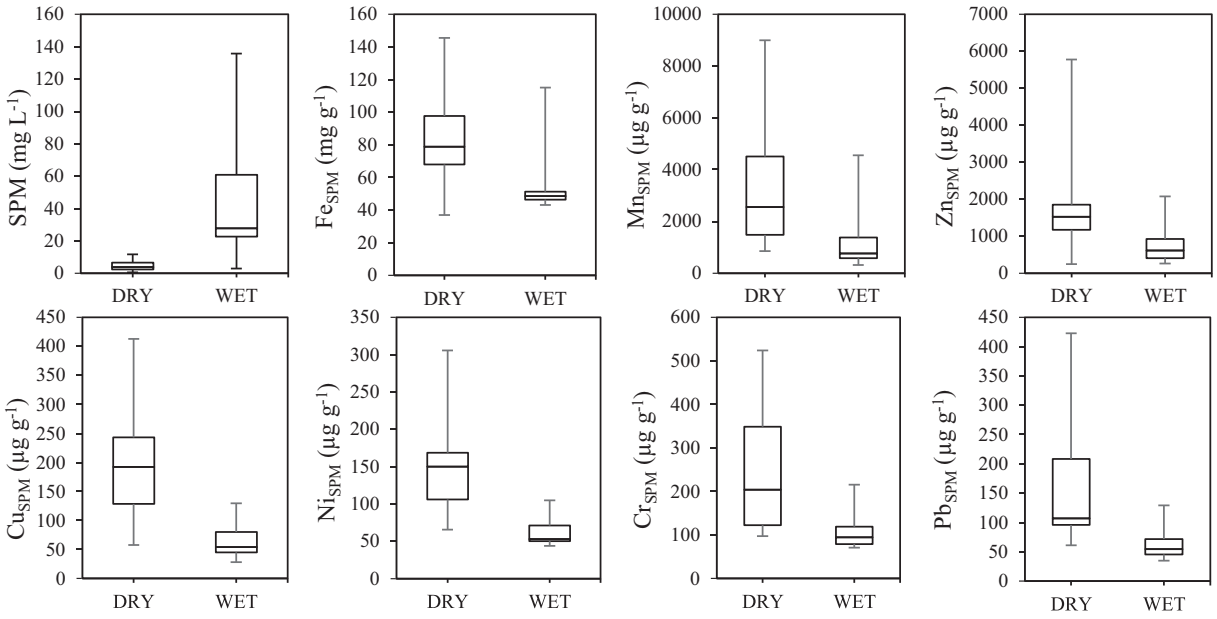

Fig. 5. Box plot summarizing suspended particle matter (SPM) concentration in water samples and metal content in SPM during the dry ($Q < 10\ m^3\ s^{-1}$) and wet ($Q > 10\ m^3\ s^{-1}$) seasons. Each box shows the 25th, 50th and 75th percentiles of median values measured at each sampling site ($N = 11$ sampling campaigns).

(Table 3). The influence of horizontal sediment transport was represented by the metal concentrations in SPM at the site just upstream (A; Table 3); in the case of D4 and D6, sediment transport from the tributaries (the Oñati and the Ego streams, respectively) was also taken into consideration. At the same time, the influence of vertical turbulence causing sediment resuspension was represented by metal concentrations in both the bulk (B; Table 3) and the fine (C; Table 3) surface sediments at the sampling site studied.

As the absolute β values indicate, horizontal sediment transport was dominant during the wet season ($Q > 10\ m^3\ s^{-1}$). In contrast, during the dry season ($Q < 10\ m^3\ s^{-1}$) metal concentrations in the SPM were more importantly dependent on metal contents in resuspended surface sediments, except at D4, D5 and D6. The findings suggest that the shallow depth of the water column due to low river discharges may cause currents to approach the bottom, resulting in stronger surface sediment resuspension. However, as the discharge in the main river notably increases through streams flowing into it and the slope of the catchment abruptly decreases from D3 (Fig. 1C), the depth of the influence zone and the velocity of the current both rise, promoting horizontal transport over surface sediment resuspension at sites downstream of D3 and the most important tributaries (D4, D5 and D6). Indeed, the outlet of the catchment (D6) is highly influenced by sediment transport from the Ego tributary in the wet season (Table 3). These results concur with the earlier interpretation of the PCA (Fig. 4) and the study by Fdez-Ortiz de Vallejuelo et al. (2017), who concluded that the SPM with the highest concentrations of Zn, Pb and Cr were collected in the Altzola gauging station during flood events as a consequence of receiving waters from the Ego tributary.

Finally, it is important to stress the need to consider particle size distribution during the surface sediment resuspension event for controlling transportation of metals towards the coastal area. In effect, during the dry season, metal concentrations in the SPM originating from sediment resuspension (B and C; Table 3) were much more dependent on metal content in the fine surface sediments (except at D5 and E1), whereas during the wet season, they depended more on the metal content in the bulk surface sediments (except at D1, D3, D6 and E2).

4. Conclusions

Recognition of the susceptibility of an urban environment due to the increasing pressure from human activity or even from climate change should encourage us to gain a deeper understanding of the environmental geochemistry of metals. Since several studies have found that environmental and human health is associated with excessive exposure to metals, and sediments act as storage and transport vectors, determining the role played by sediment particle size is a valuable tool for accurately evaluating the mobilization, deposition and dispersion of potentially toxic metals in urban ecosystems.

In this study, the use of non-destructive techniques (XRD, IR and SEM-ED spectroscopies) and invasive procedures (pseudo-total and sequential metal extraction methodologies) to analyse both bulk (<2 mm) and fine (<63 μm) surface sediments has allowed us to assess the potential environmental and health implications of metal geochemistry in an urban catchment. We observed that the composition and properties of each particle size influence the availability, and by extension, the toxicity of metals in surface sediments; the fine fraction mobilized not only higher metal pseudo-contents but also greater available metal percentages. In addition to the larger surface area per unit mass and the high content of clay minerals such as illite, mainly Fe and Mn oxyhydroxides have been found to encourage adsorption of metal on the smallest sediment particles, especially for Pb, Ni and Zn. In addition, we have demonstrated that discharges of IWW, UWW and even effluents from WWTPs along the Deba River catchment were the main anthropogenic sources of available metals in surface sediments. In the case of the bulk fraction, the origin of the metals was predominantly lithogenic and due to water erosion, which was identified as the dominant geomorphological force, was responsible for the presence of high available metals mainly at the headwater of the main river.

Finally, since each fraction represents different available metal loading, by evaluating sediment dynamics during different hydrological conditions, we were able to identify the season posing the highest ecological risk. While the resuspension of fine surface sediments notably induced significantly higher metal concentrations in SPM during dry season, resuspension of bulk surface sediments and, fundamentally, downstream transport of SPM became more relevant and diminished the ecological risk during the wet season. This knowledge will be crucial for sustainable development of an urban ecosystem in the context of climate change, given that future hydrological scenarios establish longer dry periods between precipitation events (IPCC, 2013), a situation in which balancing the intense expansion of human activities with the increasingly adverse natural conditions will be a very challenging task.

Table 3
Derived equations for metal content (Me = Fe, Mn, Zn, Cu, Ni, Cr or Pb) in suspended particulate matter ($[Me]_{SPM}$) at each sampling site when metal concentration in suspended particulate matter from upstream site(s) and concentration in the bulk ($[Me]_{BSS}$) and the fine surface sediments ($[Me]_{FSS}$) are used as independent variables. Concentrations are expressed in μg g^{-1} for all metals, except for Fe (mg g^{-1}). The independent variable with the highest influence on the dependent variable (β absolute value) is shown in bold.

Season	Equation	R^2	β values		
	A = Log $[Me]_{UPSTREAM\_SPM}$; B = Log $[Me]_{BSS}$; C = Log $[Me]_{FSS}$		A	B	C
D1					
Dry	$Log\,[Me]_{SPM} = 0.66–0.28B_{D1} + 1.36C_{D1}$	0.94	*	−0.31	**1.27**
Wet	$Log\,[Me]_{SPM} = 0.56 + 0.35B_{D1} + 0.67C_{D1}$	0.99	*	0.38	**0.62**
D2					
Dry	$Log\,[Me]_{SPM} = 0.028 + 0.18A_{D1} + 0.32B_{D2} + 0.63C_{D2}$	0.99	0.16	0.32	**0.56**
Wet	$Log\,[Me]_{SPM} = -0.032 + 0.61A_{D1} + 0.24B_{D2} + 0.066C_{D2}$	0.94	**0.65**	0.28	0.07
D3					
Dry	$Log\,[Me]_{SPM} = 0.24 + 0.47A_{D2}–0.14B_{D3} + 0.68C_{D3}$	1.0	0.43	−0.15	**0.71**
Wet	$Log\,[Me]_{SPM} = 0.15 + 0.65A_{D2} + 0.039B_{D3} + 0.27C_{D3}$	1.0	**0.62**	0.050	0.35
D4					
Dry	$Log\,[Me]_{SPM} = -0.13 + 0.61A_{D3} + 0.32A_{O1}–0.001B_{D4} + 0.15C_{D4}$	0.99	**0.54** (D3) 0.35 (O1)	0.000	0.12
Wet	$Log\,[Me]_{SPM} = -0.073 + 0.98A_{D3} + 0.29A_{O1}–0.19B_{D4}–0.042C_{D4}$	0.99	**0.92** (D3) 0.32 (O1)	−0.20	−0.044
D5					
Dry	$Log\,[Me]_{SPM} = 0.92 + 1.7A_{D4}–0.80B_{D5}–0.36C_{D5}$	0.95	**1.9**	−0.68	−0.35
Wet	$Log\,[Me]_{SPM} = -0.33 + 0.78A_{D4} + 0.43B_{D5} + 0.066C_{D5}$	0.99	**0.62**	0.33	0.057
D6					
Dry	$Log\,[Me]_{SPM} = 0.10 + 0.42A_{D5} + 0.34A_{E2} + 0.14B_{D6} + 0.22C_{D6}$	0.99	**0.38** (D5) 0.36 (E2)	0.14	0.19
Wet	$Log\,[Me]_{SPM} = -0.86 -0.47A_{D5} + 1.1A_{E2} + 0.21B_{D6} + 0.86C_{D6}$	0.99	−0.40 (D5) **0.63** (E2)	0.18	0.63
E1					
Dry	$Log\,[Me]_{SPM} = 0.92 + 0.59B_{E1} + 0.090C_{E1}$	0.98	*	**0.90**	0.12
Wet	$Log\,[Me]_{SPM} = 0.47 + 0.54B_{E1} + 0.37C_{E1}$	0.92	*	**0.65**	0.39
E2					
Dry	$Log\,[Me]_{SPM} = -0.30 + 0.082A_{E1} + 0.049B_{E2} + 1.1C_{E2}$	0.99	0.053	0.046	**0.93**
Wet	$Log\,[Me]_{SPM} = 0.39 + 1.0A_{E1}–0.11B_{E2}–0.19C_{E2}$	0.93	**1.3**	−0.16	−0.26

*Sampling location at the headwater of the stream.

Supplementary data to this article can be found online at https://doi.org/10.1016/j.scitotenv.2018.07.172.

Acknowledgements

The authors wish to thank the Ministry of Economy and Competitiveness (CTM2014-55270-R), the Basque Government (Consolidated Group of Hydrogeology and Environment, IT1029-16) and the University of the Basque Country (UPV-EHU, UFI11/26) for supporting this research.

References

Adamiec, E., Jarosz-Krzemińska, E., Wieszala, R., 2016. Heavy metals from non-exhaust vehicle emissions in urban and motorway road dusts. Environ. Monit. Assess. 188 (369), 10–11. https://doi.org/10.1007/s10661-016-5377-1.

APHA-AWWA-WPCF (American Public Health Association, American Water Works Association & Water Pollution Control Federation), 1999. Standard Methods for the Examination of Water and Wastewater. Am. Public Assoc., Washington, DC. Available online at:. https://www.mwa.co.th/download/file_upload/SMWW_1000-3000.pdf.

Apitz, S.E., 2012. Conceptualizing the role of sediment in sustaining ecosystem services: sediment-ecosystem regional assessment (SEcoRA). Sci. Total Environ. 415, 9–30. https://doi.org/10.1016/j.scitotenv.2011.05.060.

Aramendia, J., Gómez-Nubla, L., Castro, K., Fdez-Ortiz de Vallejuelo, S., Arana, G., Maguregui, M., Baonza, V.G., Medina, J., Rull, F., Madariaga, J.M., 2018. Overview of the techniques used for the study of non-terrestrial bodies: proposition of novel non-destructive methodology. Trend. Anal. Chem. 98, 36–46. https://doi.org/10.1016/j.trac.2017.10.018.

Armitage, P.D., Bowes, M.J., Vincent, H.M., 2007. Long-term changes in macroinvertebrate communities of a heavy metal polluted stream: the river Nent (Cumbria, UK) after 28 years. River Res. Appl. 23, 997–1015. https://doi.org/10.1002/rra.1022.

Bartoli, G., Papa, S., Sagnella, E., Fioretto, A., 2012. Heavy metal content in sediments along the Calore river: relationships with physical–chemical characteristics. J. Environ. Manag. 91, S9–S14. https://doi.org/10.1016/j.jenvman.2011.02.013.

Burghardt, W., 1994. Soils in urban and industrial environments. J. Soil Sci. Plant Nutr. 157, 205–214. https://doi.org/10.1002/jpln.19941570308.

Buzier, R., Tusseau-Vuillemin, M.-H., Keirsbulck, M., Mouchel, J.-M., 2011. Inputs of total and labile trace metals from wastewater treatment plants effluents to the Seine River. Phys. Chem. Earth 36, 500–505. https://doi.org/10.1016/j.pce.2008.09.003.

Campana, O., Simpson, S.L., Spadaro, D.A., Blasco, J., 2012. Sub-lethal effects of copper to benthic invertebrates explained by sediment properties and dietary exposure. Environ. Sci. Technol. 46, 6835–6842. https://doi.org/10.1021/es2045844.

Carey, R.O., Hochmuth, G.J., Martínez, C.J., Boyer, T.H., Dukes, M.D., Toor, G.S., Cisar, J.L., 2013. Evaluating nutrient impacts in urban watersheds: challenges and research opportunities. Environ. Pollut. 173, 138–149. https://doi.org/10.1016/j.envpol.2012.10.004.

Chiprés, J.A., Castro-Larragoitia, J., Monroy, M.G., 2009. Exploratory and spatial data analysis (EDA-SDA) for determining regional background levels and anomalies of potentially toxic elements in soils from Catorse-Matehuala, Mexico. Appl. Geochem. 24, 1579–1589. https://doi.org/10.1016/j.apgeochem.2009.04.022.

da Silva Oliveira, A., Bocio, A., Beltramini Trevilato, T.M., Magosso Takayanagui, A.M., Domingo, J.L., Segura-Muñoz, S.I., 2007. Heavy metals in untreated/treated urban effluent and sludge from a biological wastewater treatment plant. Environ. Sci. Pollut. Res. 14 (7), 483–489. https://doi.org/10.1065/espr2006.10.355.

Darwish, M.A.G., 2017. Stream sediment geochemical patterns around an ancient gold mine in the Wadi El Quleib area of the Allaqui region, south Eastern Desert of Egypt: implications for mineral exploration and environmental studies. J. Geochem. Explor. 175, 156–175. https://doi.org/10.1016/j.gexplo.2016.10.010.

Davutluoglu, O.I., Seckin, G., Ersu, C.B., Yilmaz, T., Sari, B., 2011. Heavy metal content and distribution in surface sediments of Seyhan River, Turkey. J. Environ. Manag. 92, 2250–2259. https://doi.org/10.1016/j.jenvman.2011.04.013.

Delshab, H., Farshchi, P., Keshavarzi, B., 2017. Geochemical distribution, fractionation and contamination assessment of heavy metals in marine sediments of the Asaluyeh port, Persian Gulf. Mar. Pollut. Bull. 115 (1–2), 401–411. https://doi.org/10.1016/j.marpolbul.2016.11.033.

Devesa-Rey, R., Díaz-Fierros, F., Barral, M.T., 2010. Trace metals in river bed sediments: an assessment of their partitioning and bioavailability by using multivariate exploratory analysis. J. Environ. Manag. 91, 2471–2477. https://doi.org/10.1016/j.jenvman.2010.06.024.

Devesa-Rey, R., Díaz-Fierros, F., Barral, M.T., 2011. Assessment of enrichment factors and grain size influence on the metal distribution in riverbed sediments (Anllóns River, NW Spain). Environ. Monit. Assess. 179, 371–388. https://doi.org/10.1007/s10661-010-1742-7.

Dung, T.T.T., Cappuyns, V., Swennen, R., Phung, N.K., 2013. From geochemical background determination to pollution assessment of heavy metals in sediments and soils. Rev. Environ. Sci. Biotechnol. 12, 335–353. https://doi.org/10.1007/s11157-013-9315-1.

Fdez-Ortiz de Vallejuelo, S., Gredilla, A., Gómez-Nubla, L., Ruiz-Romera, E., Zabaleta, A., Madariaga, J.M., 2017. Portable laser induced breakdown spectrometry to characterize the environmental impact of potentially hazardous elements of suspended particulate matter transported during a storm event in an urban river catchment. Microchem. J. 135, 171–179. https://doi.org/10.1016/j.microc.2017.09.002.

Filipek, L.H., Owen, R.M., 1979. Geochemical associations and grain-size partitioning of heavy metals in lacustrine sediments. Chem. Geol. 26 (1–2), 105–117. https://doi.org/10.1016/0009-2541(79)90033-0.

Ghanem, S.K., 2018. The relationship between population and the environment and its impact on sustainable development in Egypt using a multi-equation model. Environ. Dev. Sustain. 20, 305–342. https://doi.org/10.1007/s10668-016-9882-8.

Gómez-Nubla, L., Aramendia, J., Fdez-Ortiz de Vallejuelo, S., Madariaga, J.M., 2013. From portable to SCA Raman devices to characterize harmful compounds contained in used black slag produced in electric arc furnace of steel industry. J. Raman Spectrosc. 44 (8), 1163–1171. https://doi.org/10.1002/jrs.4342.

Gu, Y.G., Lin, Q., Yu, Z.L., Wang, X.N., Ke, C.L., Ning, J.J., 2015. Speciation and risk of heavy metals in sediments and human health implications of heavy metals in edible nekton in Beibu Gulf, China: a case study of Qinzhou Bay. Mar. Pollut. Bull. 101, 852–859. https://doi.org/10.1016/j.marpolbul.2015.11.019.

Gupta, S., Nayek, S., Saha, R.N., 2010. Temporal changes and depth wise variations in pit pond hydrochemistry contaminated with industrial effluents with special emphasis

on metal distribution in water–sediment system. J. Hazard. Mater. 183, 125–131. https://doi.org/10.1016/j.hazmat.2010.06.125.
Guven, D.E., Akinci, G., 2013. Effect of sediment size on bioleaching of heavy metals from contaminated sediments of Izmir Inner Bay. J. Environ. Sci. 25, 1784–1794. https://doi.org/10.1016/s1001-0742(12)60198-3.
Hardy, M., Cornu, S., 2006. Location of natural trace elements in silty soils using particle-size fractionation. Geoderma 133, 295–308. https://doi.org/10.1016/j.geoderma.2005.07.015.
Harmsen, J., 2007. Measuring bioavailability: from a scientific approach to standard methods. J. Environ. Qual. 36, 1420–1428. https://doi.org/10.2134/jeq2006.0492.
Horowitz, A.J., 1991. A Primer on Sediment-Trace Element Chemistry. 2nd Edition. Lewis Publishers, Chelsea, MI.
Ikem, A., Egiebor, O.N., Nyavor, K., 2003. Trace elements in water, fish and sediment from Tuskegee Lake, southern USA. Water Air Soil Pollut. 149, 51–75. https://doi.org/10.1023/A:1025694315763.
International Council for the Exploration of the Sea (ICES), 2011. Sediment dynamics in relation to sediment trend monitoring. ICES Cooperative Research Report, No. 308 (34 pp).
IPCC (Intergovernamental Panel on Climate Change), 2013. Climate change 2013. In: Stocker, T.F., Qin, D., Plattner, G.K., Tignor, M.M.B., Allen, S.K., Boschung, J., Nauels, A., Xia, Y., Bex, V., Midgley, P.M. (Eds.), The Physical Science Basis. Contribution of Working Group I Contribution to the Fifth Assessment Report of the Intergovernmental Panel on Climate Change. University Press, Cambridge, United Kingdom and New York, NY, USA Available online at:. http://ipcc.ch (1535 pp. (on 5th February)).
Jiao, X., Teng, Y., Zhan, Y., Wu, J., Lin, X., 2015. Soil heavy metal pollution and risk assessment in Shenyang Industrial District, Northeast China. PLoS One 10 (5), e0127736. https://doi.org/10.1371/journal.pone.0127736.
Kang, X., Song, J., Yuand, H., Duan, L., Li, X., Li, N., Liang, X., Qu, B., 2017. Speciation of heavy metals in different grain sizes of Jiaozhou Bay sediments: bioavailability, ecological risk assessment and source analysis on a centennial timescale. Ecotoxicol. Environ. Saf. 143, 296–306. https://doi.org/10.1016/j.ecoenv.2017.05.036.
Kirkwood, C., Everett, P., Ferreira, A., Lister, B., 2016. Stream sediment geochemistry as a tool for enhancing geological understanding: an overview of new data from south west England. J. Geochem. Explor. 163, 28–40. https://doi.org/10.1016/j.gexplo.2016.01.010.
Lanno, R., Wells, J., Conder, J., Bradham, K., Basta, N., 2004. The bioavailability of chemicals in soil for earthworms. Ecotoxicol. Environ. Saf. 57, 39–47. https://doi.org/10.1016/j.ecoenv.2003.08.014.
Lapworth, D.J., Knights, K.V., Key, R.M., Johnson, C.C., Ayoade, E., Adekanmi, M.A., Arisekola, T.M., Okunlola, O.A., Backman, B., Eklund, M., Everett, P.A., Lister, R.T., Ridgway, J., Watss, M.J., Kemp, S.J., Pitfield, P.E.J., 2012. Geochemical mapping using stream sediments in west-central Nigeria: implications for environmental studies and mineral exploration in West Africa. Appl. Geochem. 27 (6), 1035–1052. https://doi.org/10.1016/j.apgeochem.2012.02.023.
Legorburu, I., Rodríguez, J.G., Borja, A., Menchaca, I., Solaun, O., Valencia, V., Galparsoro, I., Larreta, J., 2013. Source characterization and spatio-temporal evolution of the metal pollution in the sediments of the Basque estuaries (Bay of Biscay). Mar. Pollut. Bull. 66, 25–38. https://doi.org/10.1016/j.marpolbul.2012.11.016.
Legret, M., Pagotto, C., 1999. Evaluation of pollutant loadings in the runoff waters from a major rural highway. Sci. Total Environ. 235, 143–150.
Liang, X., Song, J., Duan, L., Yuan, H., Li, X., Li, N., Qu, B., 2018. Metals in size-fractionated core sediments of Jiaozhou Bay, China: records of recent anthropogenic activities and risk assessments. Mar. Pollut. Bull. 127, 198–206. https://doi.org/10.1016/j.marpolbul.2017.12.011.
Ma, B., Cao, Y., Jia, Y., 2017. Feldspar dissolution with implications for reservoir quality in tight gas sandstones: evidence from the Eocene Es4 interval, Dongying Depression, Bohai Bay Basin, China. J. Pet. Sci. Eng. 150, 74–84. https://doi.org/10.1016/j.petrol.2016.11.026.
Mahbub, P., Ayoko, G.A., Goonetilleke, A., Egodawatta, P., 2011. Analysis of the build-up of semi and non volatile organic compounds on urban roads. Water Res. 45, 2835–2844. https://doi.org/10.1016/j.watres.2011.02.033.
Mali, M., Dell'Anna, M.M., Mastrorilli, P., Damiani, L., Ungaro, N., Belviso, C., Fiore, S., 2015. Are conventional statistical techniques exhaustive for defining metal background concentrations in harbour sediments? A case study: the coastal area of Bari (Southeast Italy). Chemosphere 138, 708–717. https://doi.org/10.1016/j.chemosphere.2015.07.046.
Martínez-Santos, M., Probst, A., García-García, J., Ruíz-Romera, E., 2015. Influence of anthropogenic inputs and a high-magnitude flood event on metal contamination pattern in surface bottom sediments from the Deba River urban catchment. Sci. Total Environ. 514, 10–25. https://doi.org/10.1016/j.scitotenv.2015.01.078.
Maslennikova, S., Larina, N., Larin, S., 2012. The effect of sediment grain size on heavy metal content. Lakes Reservoirs Ponds 6 (1), 43–54.
McGrane, S.J., Tetziaff, D., Soulsby, C., 2014. Application of a linear regression model to assess the influence of urbanised areas and grazing pastures on the microbiological quality of rural streams. Environ. Monit. Assess. 186, 7141–7155. https://doi.org/10.1007/s10661-014-3916-1.
Meaurio, M., Zabaleta, A., Uriarte, J.A., Srinivasan, R., Antigüedad, I., 2015. Evaluation of SWAT models performance to simulate streamflow spatial origin. The case of a small forested watershed. J. Hydrol. 525, 326–334. https://doi.org/10.1016/j.jhydrol.2015.03.050.
Morelli, G., Gasparon, M., Fierro, D., Hu, W.P., Zawadzki, A., 2012. Historical trends in trace metal and sediment accumulation in intertidal sediments of Moreton Bay, southeast Queensland, Australia. Chem. Geol. 300-301, 152–164. https://doi.org/10.1016/j.chemgeo.2012.01.023.
Naji, A., Ismail, A., Ismail, A.R., 2010. Chemical speciation and contamination assessment of Zn and Cd by sequential extraction in surface sediment of Klang River, Malaysia. Microchem. J. 95, 285–292. https://doi.org/10.1016/j.microc.2009.12.015.
Ong, S.A., Toorisaka, E., Hirata, M., Hano, T.A., 2010. Adsorption and toxicity of heavy metals on activated sludge. ScienceAsia 36, 204–209. https://doi.org/10.2306/scienceasia1513-1874.2010.36.204.
Palleiro, L., Rodríguez-Blanco, M.L., Taboada-Castro, M.M., Taboada-Castro, M.T., 2013. The influence of discharge, pH, dissolved organic carbon, and suspended solids on the variability of concentration and partitioning of metals in a rural catchment. Water Air Soil Pollut. 224 (1651), 1–11. https://doi.org/10.1007/s11270-013-1651-9.
Paramasivam, K., Ramasamy, V., Suresh, G., 2015. Impact of sediment characteristics on the heavy metal concentration and their ecological risk level of surface sediments of Vaigai river, Tamilnadu, India. Spectrochim. Acta A Mol. Biomol. Spectrosc. 137, 397–407. https://doi.org/10.1016/j.saa.2014.08.056.
Pascaud, G., Boussen, S., Soubrand, M., Joussein, E., Fondaneche, P., Abdeljaouad, S., Bril, H., 2015. Particulate transport and risk assessment of Cd, Pb and Zn in a Wadi contaminated by runoff from mining wastes in a carbonated semi-arid context. J. Geochem. Explor. 152, 27–36. https://doi.org/10.1016/j.gexplo.2015.01.009.
Ramirez, M., Massolo, S., Frache, R., Correa, J.A., 2005. Metal speciation and environmental impact on sandy beaches due to El Salvador copper mine, Chile. Mar. Pollut. Bull 50, 62–72. https://doi.org/10.1016/j.marpolbul.2004.08.010.
Reimann, C., De Caritat, P., 2005. Distinguishing between natural and anthropogenic sources for elements in the environment: regional geochemical surveys versus enrichment factors. Sci. Total Environ. 337, 91–107. https://doi.org/10.1016/j.scitotenv.2004.06.011.
Rule, K.L., Comber, S.D.W., Ross, D., Thornton, A., Makropoulos, C.K., Rautiu, R., 2006. Diffuse sources of heavy metals entering an urban wastewater catchment. Chemosphere 63, 64–72. https://doi.org/10.1016/j.chemosphere.2005.07.052.
Saeedi, M., Hosseinzadeh, M., Jamshidi, A., Pajooheshfar, S.P., 2009. Assessment of heavy metals contamination and leaching characteristics in highway side soils, Iran. Environ. Monit. Assess. 151 (1–4), 231–241. https://doi.org/10.1007/s10661-008-0264-z.
Saeedi, M., Li, L.Y., Karbassi, A.R., Zanjani, A.J., 2013. Sorbed metals fractionation and risk assessment of release in river sediment and particulate matter. Environ. Monit. Assess. 185, 1737–1754. https://doi.org/10.1007/s10661-012-2664-3.
Saleem, M., Iqbal, J., Shah, M.H., 2015. Geochemical speciation, anthropogenic contamination, risk assessment and source identification of selected metals in freshwater sediments-a case study from Mangla Lake, Pakistan. Environ. Nanotechnol. Monit. Manag. 4, 27–36. https://doi.org/10.1016/j.enmm.2015.02.002.
Saracoglu, S., Soylak, M., Elci, L., 2009. Extractable trace metals content of dust from vehicle air filters as determined by sequential extraction and flame atomic absorption spectrometry. J. AOAC Int. 92 (4), 1196–1202.
Simpson, S.L., Batley, G.E., 2009. Predicting metal toxicity in sediments: a critique of current approaches. Integr. Environ. Assess. Manag. 3 (1), 18–31. https://doi.org/10.1002/ieam.5630030103.
Skeries, K., Jamieson, H., Falck, H., Paradis, S., Day, S., 2017. Geochemical and mineralogical controls on metal(loid) dispersion in streams and stream sediments in the Prairie Creed district, NWT. Geochem. Explor. Environ. Anal. 17 (1), 1–19. https://doi.org/10.1144/geochem2015-375.
Song, Y., Li, F., Yang, Z., Ayoko, G.A., Frost, R.L., Ji, J., 2012. Diffusive reflectance spectroscopy for monitoring potentially toxic elements in the agricultural soils of Changjang River Delta, China. Appl. Clay Sci. 64, 75–83. https://doi.org/10.1016/j.clay.2011.09.010.
Sörme, L., Lagerkvist, R., 2002. Sources of heavy metals in urban wastewater in Stockholm. Sci. Total Environ. 298, 131–145. https://doi.org/10.1016/S0048-9697(02)00197-3.
Strom, D., Simpson, S.L., Batley, G.E., Jolley, D.F., 2011. The influence of sediment particle size and organic carbon on toxicity of copper to benthic invertebrates in oxic/suboxic surface sediments. Environ. Toxicol. Chem. 30, 1599–1610. https://doi.org/10.1002/etc.531.
Sungur, A., Soylak, M., Ozcan, H., 2014. Investigation of heavy metal mobility and availability by the BCR sequential extraction procedure: relationship between soil properties and heavy metal availability. Chem. Speciat. Bioavailab. 26 (4), 219–230. https://doi.org/10.3184/095422914X14147781158674.
Szramek, K., Walter, L.M., Kanduč, T., Ogrinc, N., 2011. Dolomite versus calcite weathering in hydrogeochemically diverse watersheds established on bedded carbonates (Sava and Soča Rivers, Slovenia). Aquat. Geochem. 17, 357–396. https://doi.org/10.1007/s10498-011-9125-4.
Terhorst, B., Ottner, F., Wriessnig, K., 2012. Weathering intensity and pedostratigraphy of the Middle to Upper Pleistocene loess/palaeosol sequence of Wels-Aschet (Upper Austria). Quat. Int. 165, 142–154. https://doi.org/10.1016/j.quaint.2011.08.042.
Tiquio, M.G.J., Hurel, C., Marmier, N., Taneez, M., Andral, B., Jordan, N., Francour, P., 2017. Sediment-bound trace metals in Golfe-Juan Bay, northwestern Mediterranean: distribution, availability and toxicity. Marine Pollut. Bull. 118, 427–436. https://doi.org/10.1016/j.marpolbul.2017.02.065.
Tüzen, M., 2003. Determination of trace metals in the River Yeşilırmak sediments in Tokat, Turkey using sequential extraction procedure. Microchem. J. 74, 105–110. https://doi.org/10.1016/S0026-265X(02)00174-1.
Unda-Calvo, J., Martínez-Santos, M., Ruiz-Romera, E., 2017. Chemical and physiological metal bioaccessibility assessment in surface bottom sediments from the Deba River urban catchment: harmonization of PBET, TCLP and BCR sequential extraction methods. Ecotoxicol. Environ. Saf. 138, 260–270. https://doi.org/10.1016/j.ecoenv.2016.12.029.
Unda-Calvo, J., Martínez-Santos, M., Ruiz-Romera, E., 2018. Implications of denitrification in the ecological status of an urban river using enzymatic activities in sediments as an indicator. J. Environ. Sci. https://doi.org/10.1016/j.jes.2018.03.037 (In Press).
United Nations, Department of Economic and Social Affairs, Population Division, 2017. World Population Prospects: The 2017 Revision, Key Findings and Advance Tables. Working Paper No. ESA/P/WP/248.
URA (Agencia Vasca del Agua - Ur Agentzia), 2004. Informe Relativo a los Artículos 5 y 6 de la Directiva Marco del Agua 2000/60/CE. Available online at:. http://www.uragentzia.euskadi.eus/informacion/articulos-5-y-6/u81-0003321/es/.

USEPA (United Sates Environmental Agency), 2001. Methods for Collection, Storage and Manipulation of Sediments for Chemical and Toxicological Analyses: 586 Technical Manual. EPA-823-B-01-002. Washington, DC. Available online at:. http://nepis.epa.gov.

USEPA (United States Environmental Agency), 1999. Protocol for Developing Sediment TMDLs. First Edition. Washington, DC. Available online at. http://nepis.epa.gov.

USEPA (United States Environmental Agency), 2007. Guidance for Evaluating the Oral Bioavailability of Metals in Soils for use in Human Health Risk Assessment, OSWER 9285, 7–80. Washington DC. Available online at:. http://nepis.epa.gov.

van Kamp, L., Leidelmeijer, K., Marsmana, G., de Hollander, A., 2003. Urban environmental quality and human well-being. Towards a conceptual framework and demarcation of concepts; a literature study. Urban Plan. 65, 5–18. https://doi.org/10.1016/S0169-2046(02)00232-3.

Violintzis, C., Arditsoglou, A., Voutsa, D., 2009. Elemental composition of suspended particulate matter and sediments in the coastal environment of Thermaikos Bay, Greece: delineating the impact of inland waters and wastewaters. J. Hazard. Mater. 66, 1250–1260. https://doi.org/10.1016/j.jhazmat.2008.12.046.

Warrier, A.K., Pednekar, H., Mahesh, B.S., Mohan, R., Gazi, S., 2016. Sediment grain size and surface textural observations of quartz grains in Late Quaternary lacustrine sediments from Schirmacher Oasis, East Antarctica: paleoenvironmental significance. Polar Sci. 10, 89–100. https://doi.org/10.1016/j.polar.2015.12.005.

Wong, C.S.C., Li, X., Thornton, I., 2006. Urban environmental geochemistry of trace metals. Environ. Pollut. 142 (1), 1–16. https://doi.org/10.1016/j.envpol.2005.09.004.

Xie, Y., Lu, G., Yang, C., Qu, L., Chen, M., Guo, C., Dang, Z., 2018. Mineralogical characteristics of sediments and heavy metal mobilization along a river watershed affected by acid mine drainage. PLoS One 13 (1), e0190010. https://doi.org/10.1371/journal.pone.0190010.

Yamagata, H., Yoshizawa, M., Minamiyama, M., 2010. Assessment of current status of zinc in wastewater treatment plants to set effluent standards for protecting aquatic organisms in Japan. Environ. Monit. Assess. 169, 67–73. https://doi.org/10.1007/s10661-009-1151-y.

Yao, Q.Z., Wang, X.J., Jian, H.M., Chen, H.T., Yu, Z.G., 2016. Behaviour of suspended particles in the Changjiang estuary: size distribution and trace metal contamination. Mar. Pollut. Bull. 103 (1–2), 159–167. https://doi.org/10.1016/j.marpolbul.2015.12.026.

Zhai, M., Kampunzu, H.A.B., Modisi, M.P., Totolo, O., 2003. Distribution of heavy metals in Gaborone urban soils (Botswana) and its relationship to soil pollution and bedrock composition. Environ. Geol. 45 (2), 171–180. https://doi.org/10.1007/s00254-003-0877-z.

Zhang, C., Wang, L., Li, G., Dong, S., 2002. Grain size effect on multi-element concentrations in sediments from the intertidal flats of Bohai Bay, China. Appl. Geochem. 17, 59–68. https://doi.org/10.1016/S0883-2927(01)00079-8.

Zhang, C., Yu, Z.G., Zeng, G.M., Jiang, M., Yang, Z.Z., Cui, F., Zhu, M.Y., Shen, L.Q., Hu, L., 2014. Effects of sediment geochemical properties on heavy metal bioavailability. Environ. Int. 73, 270–281. https://doi.org/10.1016/j.envint.2014.08.010.

Zhao, M.-Y., Zheng, Y.-F., 2014. Marine carbonate records of terrigenous input into Paleotethyan seawater: geochemical constraints from Carboniferous limestones. Geochim. Cosmochim. Acta 141, 508–531. https://doi.org/10.1016/j.gca.2014.07.001.

Zhao, M.Y., Zheng, Y.F., 2015. The intensity of chemical weathering: geochemical constraints from marine detrital sediments of Triassic age in South China. Chem. Geol. 391, 111–122. https://doi.org/10.1016/j.chemgeo.2014.11.004.

Zhou, X., Li, A., Jiang, F., Lu, J., 2015. Effects of grain size distribution on mineralogical and chemical compositions: a case study from size-fractional sediments of the Huanghe (Yellow River) and Changjiang (Yangtze River). Geol. J. 50, 414–433. https://doi.org/10.1002/gj.2546.